Progress In Electromagnetics Research, Vol. 143, 709–743, 2013

THREE-PARAMETER ELLIPTICAL APERTURE DISTRIBUTIONS FOR SUM AND DIFFERENCE ANTENNA PATTERNS USING PARTICLE SWARM OPTIMIZATION

Arthur Densmore and Yahya Rahmat-Samii*

Department of Electrical Engineering, University of California, Los Angeles, Los Angeles, CA 90095-1594, USA

Abstract—This paper presents a unified analysis of the three-parameter aperture distributions for both sum and difference antenna patterns, suitable for communications or telemetry applications with either a stationary or tracking antenna, and with the parameters automatically determined by Particle-Swarm Optimization (PSO). These distributions can be created, for example, by reflector, phased array, or other antenna systems. The optimizations involve multiple objectives, for which Pareto efficiency concepts apply, and are accelerated by compact, analytical closed-form equations for key metrics of the distributions, including the far-field radiation pattern and detection slope of the difference pattern. The limiting cases of the three-parameter distributions are discussed and shown to generalize other distributions in the literature. A derivation of the generalized vector far fields provides the background for the distribution study and helps clarify the definition of cross-polarization in the far-field. Examples are given to show that the three-parameter (3P) distributions meet a range of system-level constraints for various applications, including a sidelobe mask for satellite ground stations and maximizing pointing error detection sensitivity while minimizing clutter from sidelobes for tracking applications. The equations for the relative angle sensitivity for the difference pattern are derived. A study of the sensitivity of the 3P parameter values is presented.

Received 31 October 2013, Accepted 27 December 2013, Scheduled 3 January 2014

* Corresponding author: Yahya Rahmat-Samii (rahmat@ee.ucla.edu).

Invited paper dedicated to the memory of Robert E. Collin.

1. INTRODUCTION

Unlike its other chapters, chapter seven of the book *Antenna Theory*, by Collin and Zucker [1], deals uniquely with antenna pattern synthesis — the determination of an antenna aperture distribution to produce a given radiation characteristic — and points out that there are many methods of antenna synthesis, each of which is developed in response to a given class of problems. This paper provides a unified method for antenna pattern synthesis for the broad classes of antennas having a single main beam, with some constraint on the sidelobe levels, and including tracking antennas. This 3P unification provides closed-form equations for key metrics associated with each aperture distribution, including the radiation patterns for both sum and difference patterns, allowing quick calculation analytically rather than by brute force integration.

An antenna's radiation characteristics are largely determined by its aperture fields, which are respectively determined by the antenna's design and construction. When a realistic, comprehensive model of aperture field distribution is available with a relatively small number of parameters, the overall antenna design process can be effectively divided into two sequential steps: first identifying an aperture distribution model that meets the given system-level design constraints (considering antenna system metrics such as beamwidth, sidelobe level, and pointing error detection sensitivity) and subsequently designing the antenna to provide the chosen aperture distribution. Ideally such a model would provide analytical relationships between the aperture parameters and the system metrics, and this paper provides those relationships as equations for the 3P distribution, generalized for sum and difference patterns. The three parameters are α, β, and c. With just a few parameters for the aperture distribution the top-level antenna system design can be completed quickly.

The 3P distribution, as originally published [2], applies only to sum patterns. Here we extend it to include difference patterns as well and analyze both the sum and difference distributions in a unified manner. The 3P distributions provide considerable flexibility, as the remainder of this paper shows: the 3P sum distribution generalizes several other distributions in the literature, including Hansen's 1P distribution [3], the parabolic 2P, and the Bickmore-Spellmire 2P: all as discussed in [2]. These other distributions are represented by limiting cases of the 3P general distribution, as discussed below. What is meant by a sum pattern is the radiation pattern from the fields in the entire aperture, all in phase (adding constructively). On the other hand, the difference pattern negates the sign of the fields on one side of the

aperture so as to cancel out the fields on the other side and produce a difference pattern null in the central direction that coincides with the sum pattern's main beam. Antenna tracking systems track the null in the difference pattern to keep the main (sum) beam peaked on the signal.

An antenna's radiation pattern is determined from the aperture fields by the field equivalence principle according to Maxwell's equations. A radiation pattern varies in shape as a function of distance from the aperture: reactive near field zone closest to the antenna, radiating near field (Fresnel zone) and radiating far-field (Fraunhofer) zone. Beyond a certain distance from the aperture, which depends on the antenna size, the radiation pattern remains effectively constant in shape. In this paper the true (infinitely distant) far-fields are considered. The radiation characteristics of taper efficiency, beamwidth, sidelobe level, and the asymptotic trend of the far-out sidelobe levels are addressed for the 3P distributions.

The 3P model assumes a planar aperture, and there are several methods by which to synthesize planar apertures, e.g., [1] Chapter 7, [3], or [4] Chapter 6, that must relate the aperture parameters to a given set of design constraints. A manual design of an aperture distribution can require considerable time, and as Hansen mentions [3] can result in a suboptimal result. An optimizer that automatically searches the available range of distribution model parameter values can significantly reduce the time and effort required to meet particular design constraints — even finding unexpected solutions that might be missed if designed manually.

Metaheuristic optimization is discussed, identifying the common methods currently in use, followed by a discussion of the fundamentals of the PSO algorithm [5–10], and several examples are given for 3P distributions designed by PSO to meet common design constraints, which can involve multiple competing factors. Multiple-objective optimization is addressed from the perspective of Pareto efficiency [9]. The PSO algorithm serves the purposes of 3P distribution design quite well, as the examples reveal.

A number of mathematical appendices are included, in which the closed form equations discussed in the body of the text are each derived, in order to make the paper more complete. The following special functions are used:

$J_v(z)$ = Bessel function of the first kind, of order v.

$I_v(z)$ = modified Bessel function of the first kind, of order v.

$H_v(z)$ = Struve function, of order v.

${}_pF_q(g_1, \ldots, g_p; h_1, \ldots, h_q; z)$ = generalized hypergeometric series.

2. CONSTRUCTING FAR-FIELDS FROM APERTURE DISTRIBUTION

In this section the aperture geometry is summarized, a set of equations that represent the vector far-fields in a general form are derived (applicable to both sum and difference, and providing insight regarding the issue of the definition of cross-polarization), basic concepts pertaining to antenna radiation patterns are presented, including directivity, and the particulars regarding both sum and difference distributions are discussed, relating the model equations presented here to real-life applications.

2.1. Aperture Geometry

Consider an elliptical aperture, representing an exit aperture of a reflector or an array antenna, with major and minor axes, a and b, centered about the origin in the xy-plane bounded by

$$\left(\frac{x}{a}\right)^2 + \left(\frac{y}{b}\right)^2 = 1 \tag{1}$$

Any point inside the planar aperture is represented by a relative radial term, t, an angle, ψ, and vector $\vec{\rho}'$.

$$\vec{\rho}' = \hat{x}x' + \hat{y}y', \text{ where } x' = at\cos\psi,\ y' = bt\sin\psi,\ t \in [0,1],\ \psi \in [0, 2\pi] \tag{2}$$

2.2. Generalized Vector Far-Fields

This section reviews the construction of the vector far-field equations for an elliptical aperture distribution. The time-convention is $\exp[j\omega t]$, where $j = \sqrt{-1}$. The real-valued aperture distribution function $Q(t, \psi)$ represents the magnitude and sign of unidirectional (e.g., x- or y-directed) aperture fields, $\vec{E}_{\text{ap}}$ and $\vec{H}_{\text{ap}}$, assuming transverse electromagnetic mode (TEM) [11], with constant aperture phase other than a possible sign reversal defined by the distribution. The assumption of TEM mode in the aperture imposes

$$\eta\vec{H}_{\text{ap}} = \hat{n} \times \vec{E}_{\text{ap}}, \tag{3}$$

where η is the free-space impedance and $\hat{n}$ the outward aperture surface normal vector — the z-axis in this paper. The aperture distribution defines the aperture fields as a function of the aperture coordinates according to (4), where $\hat{p}$ is the polarization orientation of the electric field in the aperture.

$$\vec{E}_{\text{ap}}(t, \psi) / \sqrt{2\eta} = \hat{p}Q(t, \psi), \tag{4}$$

The Schelkunoff field equivalence theorem [12] relates the aperture field, given by the distribution, to equivalent electric and magnetic currents tangential to the aperture and related to vector potentials. The vector potentials then determine the radiating far-fields associated with the given aperture distribution. The equivalent currents relate to the aperture fields by the following equations.

$$\vec{J}_{eq} = \hat{n} \times \vec{H}_{\text{ap}} \quad \text{and} \quad \vec{M}_{eq} = -\hat{n} \times \vec{E}_{\text{ap}} \tag{5}$$

Following (6-95), (6-101), and (6-102) from [11], the radiated electric far-field, $\vec{E}_{ff}$, is proportional to the magnetic and electric vector potentials as given by the equations below, where the magnetic vector potential in the far-field is A_{ff}, the electric vector potential F_{ff}, μ free-space permeability, ε free-space permittivity, $k = 2\pi/\lambda$, λ is the wavelength, and ds' the elemental aperture surface area. The vector from the origin in the center of the aperture to a given far-field observation point is $\vec{r}(r, \theta, \phi)$, with corresponding unit vector $\hat{r}$.

$$\vec{E}_{ff} = \vec{E}_{Aff} + \vec{E}_{Fff} \approx \left[\hat{\theta}\hat{\theta} \cdot + \hat{\phi}\hat{\phi}\cdot\right] j\omega \left(-\vec{A}_{ff} + \eta\, \hat{r} \times \vec{F}_{ff}\right), \tag{6}$$

where

$$\vec{A}_{ff} = \frac{\exp\left[-jkr\right]}{4\pi r} \mu \iint \vec{J}_{eq} \exp\left[jk(\vec{\rho}' \cdot \hat{r})\right] ds', \tag{7}$$

and

$$\vec{F}_{ff} = \frac{\exp\left[-jkr\right]}{4\pi r} \varepsilon \iint \vec{M}_{eq} \exp\left[jk\left(\vec{\rho}' \cdot \hat{r}\right)\right] ds'. \tag{8}$$

These equations reduce in the far-field to

$$\begin{aligned} \vec{E}_{ff} \;=\; & \frac{jk \exp\left[-jkr\right]}{4\pi r} \left[\hat{\theta}\hat{\theta} \cdot + \hat{\phi}\hat{\phi}\cdot\right] \iint \left[\eta \left(-\hat{n} \times \vec{H}_{\text{ap}}\right)\right. \\ & \left. + \hat{r} \times \left(-\hat{n} \times \vec{E}_{\text{ap}}\right)\right] \exp\left[jk(\vec{\rho}' \cdot \hat{r})\right] ds'. \end{aligned} \tag{9}$$

Working out the math for the two primary polarizations yields a conditional equation:

$$\begin{aligned} & \frac{\vec{E}_{ff}}{\sqrt{2\eta}} = \frac{jk \exp\left[-jkr\right]}{4\pi r} (1 + \cos\theta)\, T \begin{cases} \hat{\theta}\cos\phi - \hat{\phi}\sin\phi, & \vec{p} = \hat{x}; \\ \hat{\theta}\sin\phi + \hat{\phi}\cos\phi, & \vec{p} = \hat{y}; \end{cases} \\ & \text{and} \quad \vec{H}_{ff} = \hat{r} \times \frac{\vec{E}_{ff}}{\eta}. \end{aligned} \tag{10}$$

Equation (10) shows that the $\hat{\theta}$ and $\hat{\phi}$ TEM spherical components of the far-field radiated from a TEM aperture are related via sine and cosine, which is a definition of a Huygens source [13] (18), for which

the Ludwig third definition of cross-polarization [14] applies. T in (10) is defined as

$$T(\theta,\phi) = \iint Q(t,\psi)\exp\left[jk(\vec{\rho}' \cdot \hat{r})\right] ds', \tag{11}$$

or

$$\begin{aligned} T(\theta,\phi) \;=\; & \int_0^{2\pi}\int_0^1 Q(t,\psi)\exp\left[jk\left(at\cos\psi\sin\theta\cos\phi\right.\right. \\ & \left.\left.+bt\sin\psi\sin\theta\sin\phi\right)\right] abt\; dtd\psi. \end{aligned} \tag{12}$$

Substituting

$$u(\theta,\phi) = kB(\phi)\sin\theta, \tag{13}$$

where

$$B(\phi) = \sqrt{a^2\cos^2\phi + b^2\sin^2\phi}, \tag{14}$$

and

$$\Phi(\phi) = \arctan\left[(b\sin\phi)/(a\cos\phi)\right], \tag{15}$$

and noting that $u(\theta, \phi)$ is the normalized radian angle, simplifies (12) to

$$T(u) = \int_0^{2\pi}\int_0^1 Q(t,\psi)\exp\left[jut\cos(\psi-\Phi)\right] abt\; dtd\psi. \tag{16}$$

In order to generalize for both sum and difference patterns, Q is defined by (17), where $R(t) \geq 0$ and n is zero for sum patterns or unity for difference patterns. $\psi = \Delta$ is the orientation of the plane perpendicular to the aperture in which the difference pattern is intended.

$$Q(t,\psi) = R(t)\cos\left[n(\psi-\Delta)\right]; \quad n = 0 \text{ or } 1 \tag{17}$$

With the help of [15] (3.915.2) (16) reduces to

$$T(u)\,|_{n=0 \text{ or } 1} = 2\pi abj^n\cos\left[n(\Delta-\Phi)\right]\int_0^1 R(t)J_n(ut)\,tdt. \tag{18}$$

The superscript *norm* is used to denote normalization by aperture area; e.g.,

$$T_S^{\text{norm}} = T_S/(\pi ab). \tag{19}$$

The above equations specify the form of the vector far-fields in spherical coordinates for a general elliptical aperture distribution Q. $n = 0$ produces a sum pattern and $n = 1$ a difference pattern. If the aperture is electrically large (yielding a pattern with a narrow beamwidth centered at $\theta = 0$) then the $(1 - \cos\theta)$ term, referred to as *element factor* of a Huygens source, can be neglected: in that case a study of the radiation patterns associated with various aperture distributions

can focus entirely on T, the radiation pattern *space factor*, and that is the path taken in this paper.

In the remainder of this paper the properties of the space factor are studied for two distinctly different types of distributions: that for producing a radiation pattern with a main beam central peak (referred to as a sum pattern and commonly used for data communications), and also that for producing a radiation pattern with a central null (referred to as a difference pattern and typically used to detect antenna pointing error for tracking). The distribution and space factor functions associated with the sum pattern type are respectively distinguished as Q_S and T_S; whereas, those for the difference pattern type as Q_D and T_D.

2.3. Radiation Pattern Characteristics

In reference to the radiation patterns there are a few terms to define. A *sum* pattern has a central peak on-axis (zero angle), and a *difference* pattern has a central null. The angular width of a sum pattern's main beam at the points where the radiated power pattern drops to half its peak value is the *half-power beamwidth*, or HPBW. A radiation pattern from an aperture with uniform phase typically has *pattern nulls* at regular angular intervals off-axis. The angular distance between the two first off-axis nulls, one on each side of the axis, is the pattern's *first-null beamwidth* (FNBW). Other than the main central beam of a sum pattern — or dual off-axis main beams of a difference pattern — the sub-beams between the off-axis nulls are the *sidelobes*, and the level of the highest sidelobe in the pattern, with respect to the level of the main beam(s), is the *peak sidelobe level* (PSLL). *Taper* (or illumination) *efficiency*, e_t, is defined by (20), which for an aperture with uniform-phase and zero crosspol is the ratio of the effective radiating area to the physical area. Zero crosspol occurs when the aperture fields, all throughout the aperture, are all oriented in the same direction, as given in (4).

$$e_t \doteq \frac{\left|\iint Q ds\right|^2}{A_{\text{ap}} \iint |Q|^2 \, ds} \tag{20}$$

Equation (14) in [2] gives the taper efficiency as the ratio of the squared magnitude of the aperture-area-normalized on-axis space factor divided by the aperture-area-normalized area integral of the square of the distribution.

Aperture *directivity* is $4\pi r^2$ times the ratio of the power radiated in one direction to the total power radiated in all directions. The

directivity is approximated in [2], for electrically large apertures, by (21), below, where P_{ap} is the total TEM aperture power.

$$D(\theta,\phi) \sim D_0 \frac{|T^{\text{norm}}|^2}{P_{\text{ap}}^{\text{norm}}} \left(\frac{1+\cos\theta}{2}\right)^2, \tag{21}$$

where

$$D_0 = \pi ab \frac{4\pi}{\lambda^2}, \tag{22}$$

and

$$P_{\text{ap}}^{\text{norm}} = \frac{P_{\text{ap}}}{\pi ab} \doteq \frac{\frac{1}{2}\iint \left|\vec{E}_{\text{ap}} \times \vec{H}_{\text{ap}}\right| ds'}{\pi ab} = \frac{\iint |Q|^2 \, ds'}{\pi ab}. \tag{23}$$

Borrowing terminology from antenna array theory, the T term in (10) is referred to as the radiation pattern's *space factor* [16], and the $(1+\cos\theta)$ term in (10) as the *element factor*, or obliquity factor, of a Huygen's source [17]. The aperture-power normalized directivity pattern of an electrically large aperture (with narrow beamwidth), for sum or difference in general, is thereby approximated by $|T^{\text{norm}}|^2/P_{\text{ap}}^{\text{norm}}$, the squared magnitude of the area-normalized space factor divided by the area-normalized aperture power.

A simple normalization is suitable to provide a basic comparison of the radiation patterns among candidate aperture distributions. Since sidelobe level with respect to the beam peak is typically one of the most significant requirements for an antenna, a suitable normalization is simply with respect to the peak of the sum pattern, so that all normalized sum patterns peak at unity (zero dB). Difference patterns, on the other hand, don't have a main beam peak: A natural alternative normalization for a difference pattern is with respect to the peak of its matching sum pattern, which places the difference pattern's dual peaks at a level of about -2 dB. The difference patterns plotted in the figures simply normalize to the pattern peak, in order emphasize the relative sidelobe levels. The matching sum pattern results from a hypothetical aperture distribution equal to the absolute value of the difference pattern's aperture distribution, and its on-axis peak value is denoted $T_{|D|}(0)$, defined in (24). $R_D(t)$ is a difference pattern's radial distribution according to (17).

$$\begin{aligned} T_{|D|}(0) &\doteq \iint |Q_D| \, ds' = \int_0^{2\pi} \int_0^1 R_D(t) \left|\cos(\psi-\Delta)\right| abt \; dtd\psi \\ &= 4ab \int_0^1 R_D(t) \, tdt \end{aligned} \tag{24}$$

Equation (25), the taper efficiency of a difference pattern, is constructed using (20), (23), and (24).

$$e_{tD} \doteq \frac{\left[T_{|D|}^{\text{norm}}(0)\right]^2}{P_{\text{ap}D}^{\text{norm}}} \tag{25}$$

One of the most important features of the difference distribution is the slope of its radiation pattern about its central null. That slope determines the sensitivity of its detection of pointing error and is the primary coefficient in any feedback tracking control system that uses the antenna pointing error detected by this slope. Equation (26) represents the slope normalized by aperture area.

$$S^{\text{norm}} \doteq \left.\frac{dT_D^{\text{norm}}(u)}{du}\right|_{u=0} \tag{26}$$

For the purpose of comparing slopes among candidate aperture distributions it's appropriate to further normalize S^{norm} by $\sqrt{P_{\text{ap}D}^{\text{norm}}}$ or $T_{|D|}^{\text{norm}}(0)$. Normalizing with respect to the square root of the area-normalized aperture power would effectively reduce the slope by the taper efficiency; whereas, the normalization of (27) by the peak of the matching sum pattern sets the (dual) peaks of all difference patterns at the same level of about $-2\,\text{dB}$ and so provides normalization independent of the taper efficiency. Bayliss [18] suggests comparing distributions by *relative angle sensitivity*, defined as normalizing by the maximum possible slope. The relative angle sensitivity, based on normalization by the matching sum pattern, is defined in (28), where $S_{\max}^{\text{normT}}$ is the maximum matching-sum-pattern-normalized angle sensitivity for the class of aperture distributions in consideration.

$$S^{\text{normT}} = S^{\text{norm}} / T_{|D|}^{\text{norm}}(0) \tag{27}$$

$$S^{\text{relative}} \doteq S^{\text{normT}} / S_{\max}^{\text{normT}} \tag{28}$$

3. SUM AND DIFFERENCE PATTERN 3P DISTRIBUTIONS

The terms 3PS and 3PD distinguish between a 3P distribution intended respectively for a sum and difference pattern.

3.1. Basic Sum and Difference Patterns

The simplest aperture distribution that produces a sum pattern is a constant, and in that case the resulting space factor T is solved with

the help of [15] (5.52.1) as

$$T_S^{\text{norm}}|_{Q_S=1} = 2\frac{J_1(u)}{u}. \tag{29}$$

The simplest elliptical aperture distribution that produces a *difference* pattern effectively involves the difference rather than the sum of the fields on either side of the aperture. Distinguishing respective sides implies the choice of a particular ϕ angle, in which phi-plane *pattern cut* the difference pattern is intended, and that angle is defined as $\phi = \Delta$. The line that divides the two halves of the aperture is at an angle perpendicular to Δ. Instead of simply negating the sign of the fields on one half of the aperture, the method given in [4] is used to create a difference pattern from a radial aperture distribution: by multiplying the radial distribution by $\cos\psi$. In this manner, the simplest example of a distribution that produces a difference pattern is a constant times $\cos\psi$, in which case (30) is the space factor for the resulting difference pattern, determined using [15] (6.561.1), where $H_0(z)$ and $H_1(z)$ are respectively the Struve functions of order zero and one.

$$T_D^{\text{norm}}|_{Q_D=\cos(\psi-\Delta)} = j\pi\cos(\Delta-\Phi)\frac{J_1(u)H_0(u) - H_1(u)J_0(u)}{u} \tag{30}$$

3.2. Sum Pattern Distributions (3PS)

The 3PS distribution, introduced in [2], is defined over an elliptical aperture, depicted in Figure 1. Each unique 3P distribution is represented by a triplet of parameter values: α, β and c. For the 3PS distributions these three parameters represent respectively: α) the *tail*

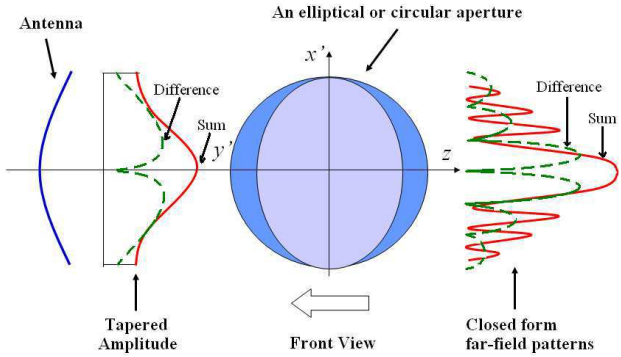

Figure 1. Elliptical aperture geometry, with generic sum and difference patterns.

shape, β) *steepness,* and c) *pedestal* height of the distribution. Each 3P distribution has a characteristic radiation pattern that is conveniently expressed by a modest closed-form equation. The fact that the 3P distribution has a closed-form radiation pattern equation provides faster convergence for any optimization algorithm that utilizes it: in each cycle of an iterative optimization the candidate three-parameter distribution is quickly evaluated (in closed-form) as the optimization algorithm proceeds. Without the closed-form equation the far-field radiation pattern of the distribution would have to be computed by numerical integration, which tends to require substantially more compute time.

The 3P sum distribution is defined in [2] as $Q(t)$ and here renamed $Q_S(t)$.

$$Q_S(t) = c + (1-c)\left(\sqrt{1-t^2}\right)^{\alpha} \frac{I_\alpha\left(\beta\sqrt{1-t^2}\right)}{I_\alpha(\beta)}, \tag{31}$$

where the domains of the three parameters (α, β, c) are $\alpha \geq 0$, $\beta \geq 0$, $0 \leq c \leq 1$. The far-field radiation integral for the 3P sum distribution is solved in closed form using [15] (6.683.2).

$$T_S^{\text{norm}}(u) = 2c\frac{J_1(u)}{u} + (1-c)\frac{2\beta^\alpha J_{\alpha+1}\left(\sqrt{u^2-\beta^2}\right)}{I_\alpha(\beta)\left(\sqrt{u^2-\beta^2}\right)^{\alpha+1}} \tag{32}$$

The asymptotic behavior of T_S for large u describes the level of the far-out sidelobes, and for the 3PS distribution that behavior is in (33). Note that for large argument, z, $J_\nu(z) \sim z^{-1/2}$.

$$T_S(u)|_{u\to\infty} \sim \begin{cases} u^{-3/2}, & c \neq 0; \\ u^{-3/2-\alpha}, & c = 0. \end{cases} \tag{33}$$

The normalization of the 3P sum distribution is discussed in [2], where the choice is made to normalize by the square root of the normalized aperture power integral. The aperture-area normalized power integral is

$$P_{\text{apS}}^{\text{norm}} = c^2 + 4c(1-c)\frac{I_{\alpha+1}(\beta)}{\beta I_\alpha(\beta)} + \frac{(1-c)^2}{2\alpha+1}\left(1 - \frac{I_{\alpha+1}^2(\beta)}{I_\alpha^2(\beta)}\right). \tag{34}$$

The limiting cases for the 3PS distribution are discussed in [2] and become the Bickmore-Spellmire distribution when $c = 0$, the parabolic 2P model when $\beta = 0$, and the 1P model when $\alpha = 0$ and $c = 0$. These three limiting cases are given respectively by (35), (36), and (37), and several example distributions for each case are displayed respectively

in Figures 2–4.

$$_{\text{B-S}}Q_S(t) = \left(\sqrt{1-t^2}\right)^{\alpha} \frac{I_\alpha\left(\beta\sqrt{1-t^2}\right)}{I_\alpha(\beta)} \tag{35}$$

$$_{\text{2P}}Q_S(t) = c + (1-c)\left(1-t^2\right)^{\alpha} \tag{36}$$

$$_{\text{1P}}Q_S(t) = \frac{I_0\left(\beta\sqrt{1-t^2}\right)}{I_0(\beta)} \tag{37}$$

Since the broad classes of antennas that the 3P distributions apply to are mainly concerned with tradeoffs between directivity and PSLL, an appreciation of the main distinctions between the three limiting cases can be obtained by considering the uniquely different tradeoff that each case provides between PSLL and FNBW/2, the angle (u) at which the first off-axis null occurs, which is an indirect measure of

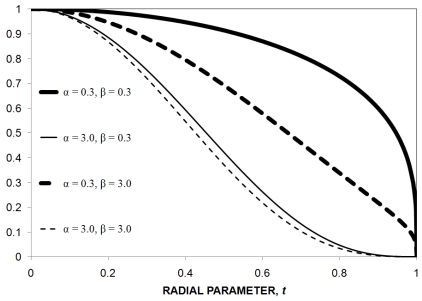

Figure 2. Example distributions for 3PS limiting case of $c = 0$.

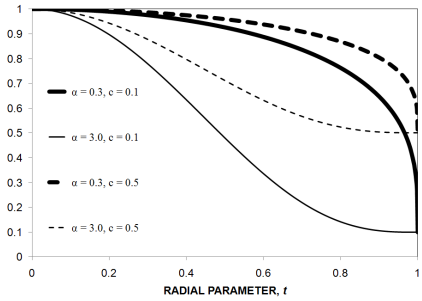

Figure 3. Example distributions for 3PS limiting case of $\beta = 0$.

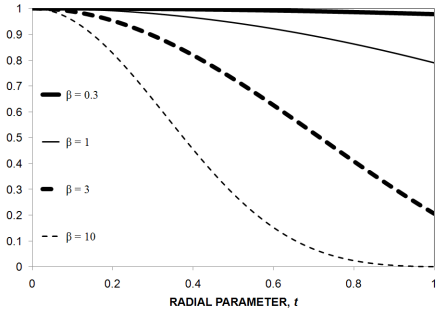

Figure 4. Example distributions for 3PS limiting case of $\alpha = c = 0$.

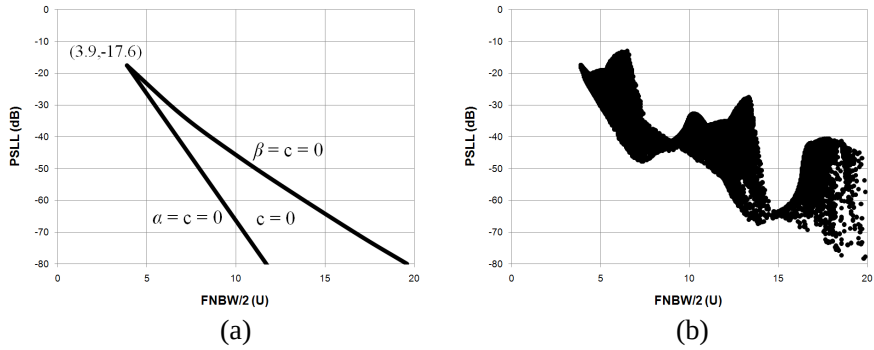

Figure 5. (a) PSLL versus FNBW/2 Pareto fronts for 3PS limiting cases of $c = 0$, $a = c = 0$, and $\beta = c = 0$. (b) PSLL versus FNBW/2 Pareto front for 3PS limiting case of $\beta = 0$.

directivity. A multi-objective optimization, such as a tradeoff between PSLL and FNBW, is effectively summarized by a Pareto front [19, 20]. Pareto fronts for the radiation patterns of these three limiting cases of the 3PS distribution are given by the perimeters of sample-populated areas presented respectively in Figures 5(a) and 5(b). The case of $c = 0$ appears as essentially a fan sector and fills the region between the curves, and that of $\beta = 0$ has particularly detailed features. For reduction of the radiation pattern (32) in the limiting case of $\beta \to 0$, note that

$$\lim_{\beta \to 0} \left[\beta^{\alpha} / I_{\alpha} (\beta) \right] = 2^{\alpha} \Gamma (\alpha + 1) . \tag{38}$$

3.3. Difference Pattern Distributions (3PD)

The most commonly referenced distribution for a difference pattern appears to be that of Bayliss [18], which presents a two-parameter circular aperture distribution as an analog to the Taylor $\bar{n}$ sum distribution [17]. Section IV in [3] references the discussion in [4] of a circular Bayliss distribution based on multiplying by $\cos\psi$. This is a natural method of producing a difference pattern, judging by the fact that the higher-order mode (HE_{21}) linearly-polarized fields in the mouth of a large corrugated horn (commonly used for detecting tracking error in satellite earth stations) have the $\cos\psi$ dependence [21]. A difference pattern distribution for a line source is suggested in [22] as a complement to the 3P sum distribution in [2]. That suggestion is basically to multiply the radial $Q(t)$ distribution in [2] by t. Heeding that suggestion, along with the $\cos\psi$ factor, the

3P difference pattern distribution reviewed in this paper for a general elliptical aperture is defined as

$$Q_D(t,\psi) \doteq \cos(\psi-\Delta)\left\{c+(1-c)t\left[Q_S(t)|_{c=0}\right]\right\}, \tag{39}$$

or

$$Q_D(t,\psi)=\cos(\psi-\Delta)\left\{c+(1-c)\,t\left(\sqrt{1-t^2}\right)^{\alpha}\frac{I_\alpha\left(\beta\sqrt{1-t^2}\right)}{I_\alpha(\beta)}\right\}. \tag{40}$$

The 3P difference pattern far-field is solved using [15] (3.915.2, 6.561.1, and 6.682.2):

$$\begin{aligned} T_D^{\text{norm}}(u) \;=\; & 2j\cos(\Delta-\Phi)\left\{c\frac{\pi}{2u}\left[J_1(u)\,H_0(u)-H_1(u)J_0(u)\right]\right. \\ & \left.+(1-c)\frac{u\beta^\alpha J_{\alpha+2}\left(\sqrt{u^2-\beta^2}\right)}{I_\alpha(\beta)\left(\sqrt{u^2-\beta^2}\right)^{\alpha+2}}\right\}. \end{aligned} \tag{41}$$

The asymptotic behavior of T for large u describes the level of the far-out sidelobes, and for the 3P difference distribution that behavior is given in (42). This is steeper than for the sum distribution when $c=0$.

$$T_D(u)|_{u\to\infty} \sim \begin{cases} u^{-3/2}, & c\neq 0; \\ u^{-5/2-\alpha}, & c=0. \end{cases} \tag{42}$$

On-axis field strength of the matching sum pattern corresponding to the absolute value of the 3PD distribution, solved using [15] (6.683.6), is

$$T_{|D|}^{\text{norm}}(0) = 2\left\{\frac{c}{\pi}+(1-c)\sqrt{\frac{2}{\pi}}\frac{I_{\alpha+3/2}(\beta)}{\beta^{3/2}I_\alpha(\beta)}\right\}. \tag{43}$$

The total aperture power in the 3PD distribution is similarly found:

$$\begin{aligned} P_{\text{ap}D}^{\text{norm}} \;=\; & \left\{\frac{c^2}{2}+\frac{2c(1-c)}{\beta^{3/2}}\sqrt{\frac{\pi}{2}}\frac{I_{\alpha+3/2}(\beta)}{I_\alpha(\beta)}+\frac{(1-c)^2}{2}\right. \\ & \left.\left[\frac{1-\dfrac{I_{\alpha+1}^2(\beta)}{I_\alpha^2(\beta)}}{2\alpha+1}-\frac{\beta^{2\alpha}{}_2F_3\left(\begin{matrix}[2\alpha+2,\,\alpha+1/2]\,; \\ [2\alpha+1,\,2\alpha+3,\,\alpha+1]\,;\end{matrix}\;\beta^2\right)}{2^{2\alpha+1}(\alpha+1)\,\Gamma^2(\alpha+1)\,I_\alpha^2(\beta)}\right]\right\} \end{aligned} \tag{44}$$

The limiting cases for the 3PD distribution that correspond to the same aforementioned cases as for 3PS, (35)–(37), are presented in (45)–(47),

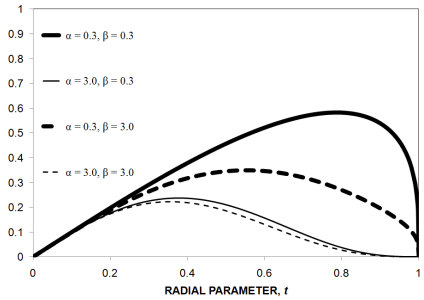

Figure 6. Example distributions for 3PD limiting case of $c = 0$.

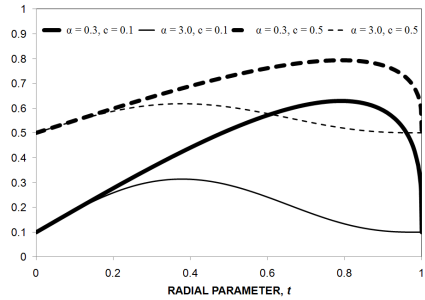

Figure 7. Example distributions for 3PD limiting case of $\beta = 0$.

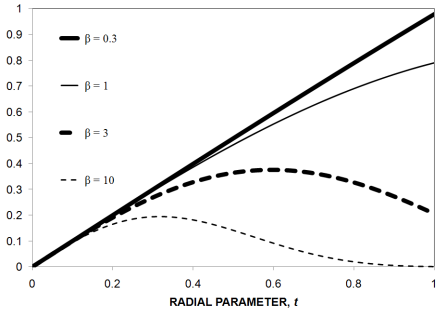

Figure 8. Example distributions for 3PD limiting case of $\alpha = c = 0$.

and example distributions for each case are displayed respectively in Figures 6–8.

$$_{c=0}R_D(t) = t\left(\sqrt{1-t^2}\right)^{\alpha}\frac{I_\alpha\left(\beta\sqrt{1-t^2}\right)}{I_\alpha(\beta)} \tag{45}$$

$$_{2\mathrm{P}}R_D(t) = c + (1-c)\,t\left(1-t^2\right)^{\alpha} \tag{46}$$

$$_{1\mathrm{P}}R_D(t) = t\frac{I_0\left(\beta\sqrt{1-t^2}\right)}{I_0(\beta)} \tag{47}$$

Pareto fronts that reveal the uniquely different tradeoff that each case provides between PSLL and FNBW are presented in Figures 9(a) and 9(b). The case of $c = 0$ appears as a fan sector, and that of $\beta = 0$ has particularly detailed features. Pareto fronts revealing the tradeoffs between PSLL and relative angle sensitivity are presented in Figures 10(a) and 10(b). The case of $c = 0$ is similar in shape to

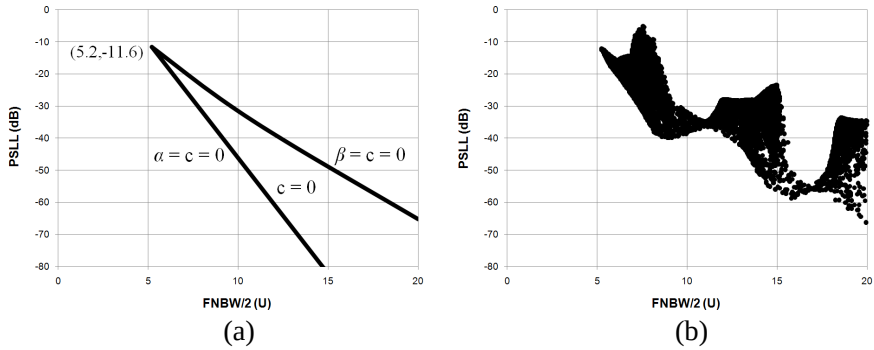

Figure 9. (a) PSLL versus FNBW/2 Pareto fronts for 3PD limiting cases of $c = 0$, $a = c = 0$, and $\beta = c = 0$. (b) PSLL versus FNBW/2 Pareto front for 3PD limiting case of $\beta = 0$.

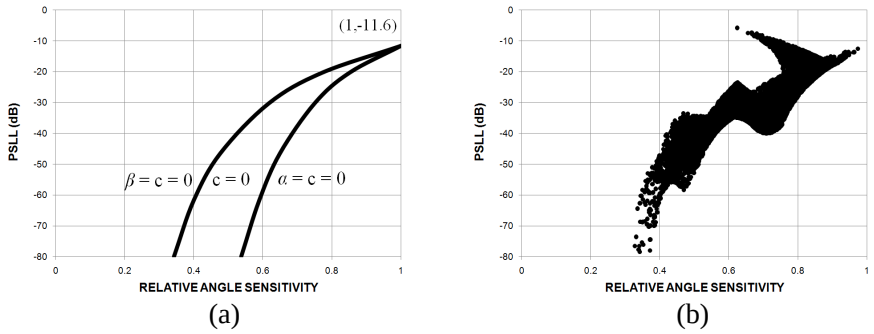

Figure 10. (a) PSLL versus relative angle sensitivity Pareto fronts for 3PD limiting cases of $c = 0$, $\alpha = c = 0$, and $\beta = c = 0$. (b) PSLL versus relative angle sensitivity Pareto front for 3PD limiting case of $\beta = 0$.

the former set of Pareto fronts; although, in Figure 10(a) what was in Figure 9(a) a nearly straight fan sector is seen to be significantly curved.

$$S^{\text{norm}} = 2j\cos(\Delta - \Phi)\left\{\frac{c}{6} + \frac{(1-c)\,I_{\alpha+2}(\beta)}{\beta^2 I_\alpha(\beta)}\right\} \tag{48}$$

The aperture area normalized slope of the 3PD pattern is presented in (48). Further normalizing by the peak of the matching sum pattern and also the maximum possible slope results in the *relative angle sensitivity* of the distribution, given in (50). The maximum matching-

sum-pattern-normalized angle sensitivity, $S_{\max}^{\text{normT}}$, for a 3PD pattern occurs in the limit as all three of the 3P parameters approach zero, in which case the 3PD distribution has a triangular shape peaking at the aperture edge.

$$S_{\max}^{\text{normT}} = \frac{\lim\limits_{\alpha=\beta=c\to 0} S^{\text{norm}}}{\lim\limits_{\alpha=\beta=c\to 0} T_{|D|}^{\text{norm}}(0)} = \frac{\sqrt{\pi}}{2}\frac{\Gamma\left(\frac{5}{2}\right)}{\Gamma(3)} \tag{49}$$

$$S^{\text{relative}} = S^{\text{normT}} \Bigg/ \left[\frac{\sqrt{\pi}}{2}\frac{\Gamma\left(\frac{5}{2}\right)}{\Gamma(3)}\right] \tag{50}$$

4. METAHEURISTIC OPTIMIZATION METHODS

Optimization techniques used in the electromagnetic engineering community are often metaheuristic because of the complexity of the tradeoffs involved. Metaheuristic methods involve stochastic optimization to distinguish global from local optimal solutions, as opposed to classical optimizers that are meant to produce exact solutions for simpler classical models with local extrema, which if applied to real-world engineering problems tend to get stuck on local optimum solutions.

A basic overview of metaheuristic methods is provided in [23]. Such methods include Ant Colony Optimization [24], Covariance Matrix Adaptation Evolution Strategy (CMA-ES) [25], Genetic Algorithms (GA) [26], Invasive Weed Optimization (IWO) [27], PSO [5–10], Simulated Annealing [28], and Tabu Search [29]. Among these optimization techniques, the PSO is a practical balance between model simplicity and robust, rapid, global solution convergence. Examples of the state of the art of the application of PSO to fractal and adaptive phased-array antennas are given in [30–32].

Optimization can pertain to a system with one or more variables with one or more optimization objectives, goals, or constraints. With only one objective the optimization can evaluate it with a fitness function. If there are multiple (competing) objectives evaluation of the optimality becomes more complicated. There are generally two approaches to multi-objective optimization: 1) combining fitness functions and 2) referring to a Pareto front [9, 19, 20]. A classical way of combining multiple objectives into a single fitness function is a weighted sum of fitness functions — one from each objective — where the result of the overall optimization can depend on the choice of weighting. An example is given in (51), which involves the two competing objectives of peak sidelobe level and first-null beamwidth. Pareto optimality represents the trade-off between multiple goals: A

solution is Pareto optimal when it is not possible to improve one goal without degrading at least one of the others. Optimization by Pareto front involves more intensive numerical investigation to determine the actual boundary of optimality between competing objectives, and a few examples of Pareto fronts are given below. In general there is no singly optimal solution to a multi-objective optimization: the set of Pareto optimal multi-objective solutions is called a Pareto front.

4.1. Particle Swarm Optimization (PSO)

The PSO algorithm is similar to the concept of a swarm of bees in a field, effectively communicating their individual findings and so guiding the swarm as a whole ever closer to a suitable location to converge upon. A PSO algorithm directs the search and evaluates a fitness function, customized for the particularly specified goal(s), to evaluate the merit of each candidate solution considered by any member of the swarm. Example PSO convergence plots are shown in Figures 11(a) and 11(b), using respective fitness functions given by (51) and (52), and each with twenty agents per swarm and thirty swarm trials per iteration. These two are comparable since they both have the same goal of −40 dB PSLL; although, one is for a sum pattern and the other for a difference pattern. Note that the convergence plot in Figure 11(a) involves a fitness function that is not conditional; whereas, that in Figure 11(b) is conditional: in the former case the average fitness is considerably larger than in the latter; although, the rate of convergence

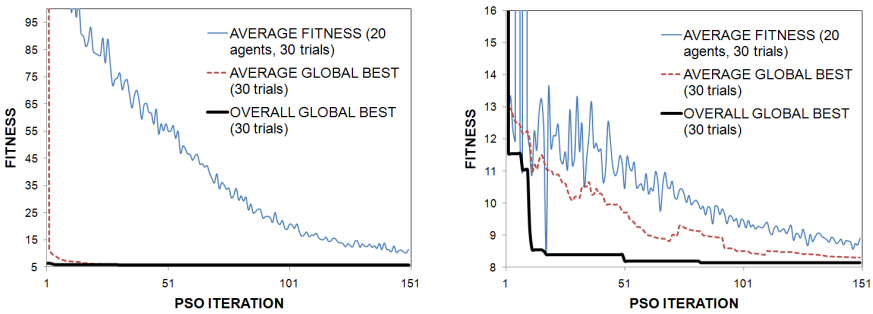

Figure 11. (a) PSO convergence for design of 3PS pattern with −40 dB PSLL and minimum FNBW. (b) PSO convergence for design of 3PD pattern with −40 dB PSLL and minimum FNBW.

appears to be a bit faster in the former than the latter.

$$\text{fitness\_11(a)} = (\text{PSLL}\,(\text{dB}) - \text{goal})^2 + \text{FNBW}\,(u)\,/2, \tag{51}$$

$$\text{fitness\_11(b)} = \begin{cases} \text{FNBW}\,(u)\,/2, & \text{if PSLL} \leq \text{goal;} \\ 999, & \text{otherwise.} \end{cases}, \tag{52}$$

The position, in model parameter space, of the search agent (swarm member) with the best fitness value among the swarm at any iteration is the *global best* for that iteration. Each search agent moves about the parameter space and its flight path is pulled toward that global best. It is also pulled toward its own *personal best* location, and its flight path is also affected by its own inertia and random motion.

Consider the flight trajectory of any particular swarm member ("search agent", or "bee") in the PSO model n-dimensional parameter space, letting $n = 2$ here for simplicity. Applying real-world physics and assuming each bee naturally counteracts the force of gravity, we imagine that each bee has some linear momentum that Newton's Law preserves until external forces are applied or the bee alters its path. External winds and individual bee behavior combine to provide a seeming randomness to the individual flight paths. By means of the waggle dance a bee communicates to its hive-mates in which direction with respect to the Sun and how far it flew to reach the food source it found. So we can imagine that each bee's flight path is affected by 1) Newton's Law, 2) random motion, 3) its own knowledge of the best place at which it has found food (personal best, or p_{best}), and 4) the best overall location found by any member of the swarm (the global best, or g_{best}). This is represented by (53) for the motion of any PSO search agent. v_n represents the search agent's velocity vector in the current (nth) iteration, x_n represents its current position vector, w is the momentum factor, c_1 and c_2 effectively represent *spring constants* pulling the search agent respectively towards its personal and the overall swarm's global best locations, and rand () is a strictly-positive valued random number function ranging between the zero and one. Δt is a discrete step representing the time between iterations.

$$\begin{aligned} x_{n+1} &= x_n + v_n \Delta t, \quad \text{and} \\ v_{n+1} &= w v_n + c_1 \text{rand}\,() \,(p_{\text{best}} - x_n) + c_2 \text{rand}\,() \,(g_{\text{best}} - x_n) \end{aligned} \tag{53}$$

5. PARTICLE SWARM OPTIMIZATION OF 3P DISTRIBUTIONS

The goal for the 3P distribution is to provide an antenna aperture distribution that provides specified radiation pattern characteristics, such as beamwidth, PSLL, taper efficiency, sidelobe level limit (mask)

as a function of angle, and for the difference pattern: relative angle sensitivity. These characteristics are translated into a fitness function for the optimizer, which by convention the PSO minimizes. Throughout the optimization process the PSO varies the 3P parameter values automatically, within any parameter value constraints imposed on the algorithm. Convergence is faster when any of the 3P parameters are constrained to within a range known to provide the desired solution.

Several examples of the application of PSO to the 3P distributions are given. Two examples of the design of 3PS distributions by PSO are presented: maximizing aperture taper efficiency while satisfying a sidelobe mask, and minimizing the beamwidth with the peak sidelobe level (PSLL) set to a target value. A study of the sensitivity of the 3P parameter values is presented, followed by examples of 3PD distributions design by PSO for a range of PSLL constraints.

5.1. Example 1: 3PS Maximum Gain with a Sidelobe Mask

The first example maximizes the gain with a sidelobe constraint. Given a uniform phase aperture, which the 3P distribution assumes, maximum gain is associated with peak taper efficiency. A formal constraint for the sidelobes of a geostationary satellite ground station antenna is the FCC 25.209 mask [33], which starts at 1.5 deg from beam peak with sidelobe directivity constraint of twenty-nine decibels isotropic gain minus twenty-five decibels times the base ten logarithm of the pattern angle in degrees (for conventional Ku- or Ka-band geostationary service ground stations). The conditional fitness

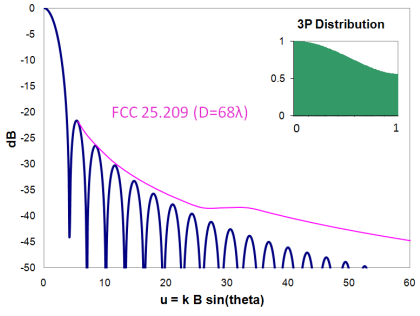

Figure 12. PSO 3PS radiation pattern achieving maximum taper efficiency while also meeting a sidelobe mask.

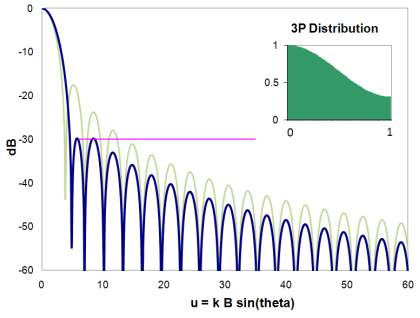

Figure 13. PSO 3PS distribution and radiation pattern achieving PSLL of −30 dB peak with minimum beamwidth.

function which PSO minimizes for this example is

$$\text{fitness\_12} = \begin{cases} -e_t, & \text{if all sidelobes below the mask;} \\ 999, & \text{otherwise.} \end{cases} \tag{54}$$

If any sidelobe exceeds the mask then the candidate 3P distribution is deemed out-of-bounds and discarded with a very large fitness value. This out-of-bounds treatment is the same as how search agents that wander outside an acceptable range of parameter values can be dealt with in the PSO algorithm by applying *invisible boundaries* [6]. Figure 12 shows the 3P distribution and radiation pattern from this PSO run, which yielded 3P parameter values of alpha = 1.9389, beta = 1.6928, and $c = 0.5581$. The locus of the sidelobe peaks is seen to follow the mask, and a 96.6% taper efficiency is achieved with an aperture diameter of 68 wavelengths.

5.2. Example 2: 3PS Minimum Beamwidth with Specified PSLL

The second example provides a 3P antenna aperture distribution that achieves a radiation pattern with sidelobe level (PSLL) less than −30 dB peak while minimizing beamwidth. For this example the fitness function is the square of the difference between the PSLL and the goal, in dB, plus the angle, u, of the first null.

$$\text{fitness\_13} = (\text{PSLL} - \text{goal})^2 + \text{FNBW}/2, \tag{55}$$

where the PSLL goal is −30 dB peak. The 3P parameters produced by one PSO run meeting these constraints are alpha = 2.002, beta = 2.877, and $c = 0.306$, and the resulting radiation pattern and 3P distribution are shown in Figure 13. This figure also superimposes (light shading) the uniform-amplitude aperture radiation pattern for comparison — in which case the sidelobes would be considerably higher than that provided by the optimized 3P distribution.

5.3. Example 3: 3PS Family of PSO Solutions

PSO typically yields a family of solutions, all of which satisfy the constraints to some degree. Figure 14 shows such a family, with a PSLL of −40 dB. The selected family of solutions is: 1) alpha = 2.2390, beta = 0.5625, $c = 0.139$, 2) alpha = 1.2196, beta = 3.7930, $c = 0.1015$, and 3) alpha = 0.6207, beta = 4.5970, $c = 0.0757$. This family represent only three of many PSO solutions that were found to meet the given requirements, and these three were chosen because of the substantial variation in their alpha parameter values, to show that the combination of a high alpha value and low beta value can provide a

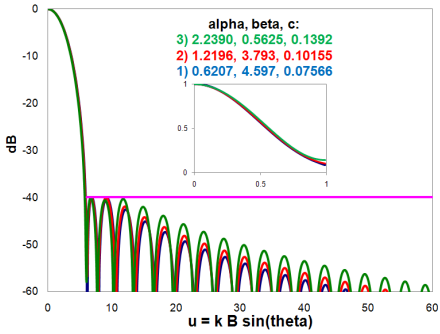

Figure 14. PSO 3PS distributions and radiation patterns for a family of PSO solutions all achieving PSLL of −40 dB peak with minimum beamwidth.

similar distribution as the combination of a low alpha value and high beta. There is little difference between the distributions of each of these family members, as the inset distribution shows (since they all meet the same design requirements). The fitness function is given by (55).

5.4. Example 4: 3P Pattern Sensitivity to Variation of Parameter Values

A practical design must account for implantation error, and so a sensitivity analysis was conducted to determine how sensitive the 3P distribution might be to variations in each of the parameter values. The first PSO family member 3PS solution in Figure 14 is used as the basis for the parameter sensitivity analysis. Figure 15(a) shows that a 10% variation in the alpha parameter value can cause as much as 5–10 dB variation in the level of the first sidelobe. Figure 15(b) shows that the beta parameter value is the least sensitive to variation of its value: only a few dB variation in the level of the first sidelobe level result from a significant variation in the beta value from −100% to +300%. Figure 15(c) shows that the 3P c-parameter has intermediate sensitivity. The level of the first sidelobe level varies several dB with a 10% variation in the value of the c-parameter value. The corresponding variations in 3PD patterns are comparable to those given here for 3PS.

5.5. Examples 5–7: 3PD Maximum Angle Sensitivity with Specified PSLL

PSO examples are presented in Figures 16(a)–(c) for 3PD distributions with PSLL design goals of respectively −30, −48 and −55 dB, while

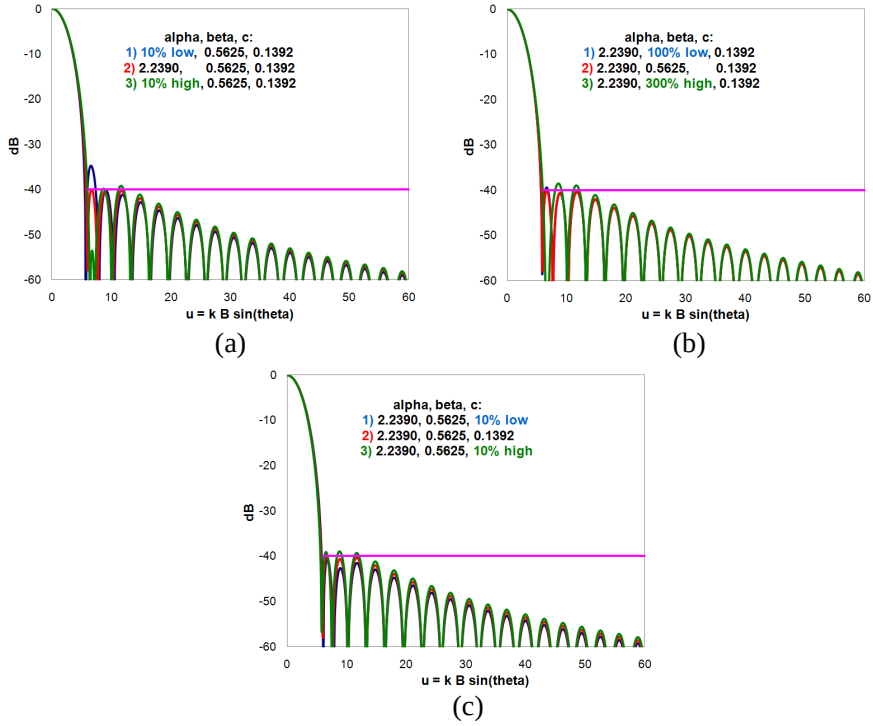

Figure 15. (a) PSO parameter sensitivity, showing variation of radiation pattern when only the 3PS *alpha* parameter value is changed from the PSO solution value by ±10%. (b) PSO parameter sensitivity, showing variation of radiation pattern when only the 3PS *beta* parameter value is changed by −100% and +300%. (c) PSO parameter sensitivity, showing variation of radiation pattern when only the 3PS c parameter value is changed from the PSO solution value by ±10%.

simultaneously maximizing the relative angle sensitivity, using the fitness function of (56). The 3P parameter values for Figure 16(a) are alpha = 1.9949, beta = 0.0194, and $c = 0.0804$, in which case a relative angle sensitivity of 79% is achieved with −30 dB PSLL. Those for Figure 16(b) are alpha = 2.3292, beta = 1.3064, and $c = 0.0460$, in which case a relative angle sensitivity of 75% is achieved with −38 dB PSLL. The 3P parameter values for Figure 16(c) are alpha = 0.0318, beta = 8.3484, and $c = 0.0031$, in which case a relative angle sensitivity of 67% is achieved with −55 dB PSLL. The 3PD distribution can meet even considerably deeper PSLL limits than given by these examples, indicated by Figure 9(a). These optimal multi-objective solutions are

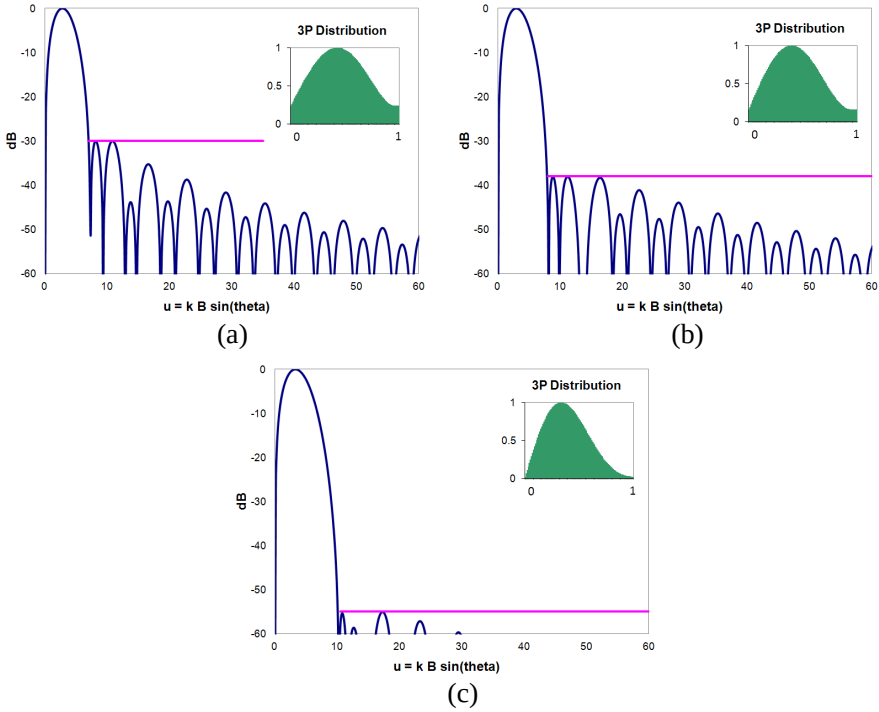

Figure 16. (a) PSO 3PD designed for −30 dB PSLL and maximum relative angle sensitivity. The inset 3PD distribution is shown normalized to its peak height. (b) PSO 3PD designed for −38 dB PSLL and maximum relative angle sensitivity. The inset 3PD distribution is shown normalized to its peak height. (c) PSO 3PD designed for −55 dB PSLL and maximum relative angle sensitivity. The inset 3PD distribution is shown normalized to its peak height.

typically found on the edge of a Pareto front. Bayliss [18] reveals that for a difference pattern to realistically achieve maximum relative angle sensitivity with a given maximum PSLL requires that its first sidelobes be of uniform level, and Figures 16(a)–(c) show that the 3PD distributions determined by PSO with those constraints have that very characteristic.

$$\text{fitness\_16} = \begin{cases} -\left(\text{relative angle sensitivity}\right), \text{ if PSLL} \leq \text{goal}; \\ 999, \text{ otherwise.} \end{cases} \tag{56}$$

6. CONCLUSION

The 3P distribution is presented for both sum and difference patterns in the context of providing a versatile amplitude distribution model of for an entire class of uniform-phase elliptical antenna apertures. Analytical closed form equations for several characteristics of a general 3PS or 3PD distribution were derived: the far-field radiation pattern, taper efficiency, aperture power, asymptotic sidelobe level, and for the 3PD also the relative angle sensitivity. The PSO algorithm was discussed, and references for other metaheuristic optimization methods were given. Several examples of designing 3P distributions by PSO demonstrate that the 3P distribution can meet a range of real-world design constraints. The PSO algorithm converges to a solution in each case with different 3P antenna aperture design constraints. Radiation patterns and distributions for a family of solutions which all satisfy the same requirements were presented, and the sensitivity of each of the 3P parameter values was investigated. The PSO optimized 3P patterns meet peak sidelobe, taper efficiency and sidelobe mask requirements. The PSO optimized 3P patterns display the ideal characteristic of uniform close-in sidelobe levels when in addition to constraining the optimization by a specified PSLL it is also additionally constrained by maximum taper efficiency, in the case of a sum pattern, or by maximize angle sensitivity in the case of a difference pattern. The versatility of the 3P distribution and PSO's utility as a metaheuristic optimizer combine to provide customized aperture distributions for a versatile range of applications.

ACKNOWLEDGMENT

Rahmat-Samii's reflection: I am delighted to contribute this paper to the special issue of PIERS dedicated to the memory of Prof. Robert E. Collin, whose contributions and services to the electromagnetic community are immeasurable. We have all benefitted from his wisdom and his technical excellence. His papers are original, mathematically detailed and always address some interesting concepts. His books have inspired and provided solid foundation for the education of numerous students worldwide. I have also tremendously enjoyed my encounters with Prof. Collin. When I was a graduate student at the University of Illinois Urban-Champaign, Prof. Collin was a guest speaker and delivered a paper on the Dyadic Green's function and its singularities. His talk inspired me to write a short paper on this subject based on the application of distribution theory and the paper has been one of my most referenced papers [34]. In 2000, Prof. Collin and I organized two millennium sessions at the IEEE Antennas and

Propagation Society Annual International Symposium held in Salt Lake City, Utah. These sessions were tremendously successful and we were able to blend some of the pioneering developments along with more recent advances. (The contributors for session I were J. Van Bladel, M. Iskander, C. Butler, M. Stuchly, Y. Rahmat-Samii, K. Warble, R. C. Hansen, J. Huang, T. Sarkar, L. Katehi and the contributors for session II were, S. Gillespie, G. Hindman, R. Collin, A. Ishimaru, H. Bertoni, T. Senior, P. Pathak, R. Harrington, A. Taflove, W. Cho. These are some of biggest names in our profession). I had a great time organizing these sessions along with Prof. Collin. It is so humbling to be able to dedicate this paper to the memory of Prof. Collin. My Ph.D. student, Arthur Densmore, and I have assembled this paper in order to provide a revisit and also enhancement of the utilization of 3-parameter (3P) aperture distributions for both sum and difference antenna patterns. In particular, the mathematical development has been made for an elliptical aperture whereby a circular aperture is a special case. Additionally the power of Particle Swarm Optimization (PSO) method is used to design some very interesting aperture distributions for various applications. It is in the spirit of Prof. Collin's research style to strive for mathematical rigor and apply it to engineering problems. I am also thankful to Prof. Weng Cho Chew for extending the invitation to contribute this paper.

APPENDIX A. MATHEMATICAL APPENDICES

A.1. Derivation of (18), the Generalized Space Factor Integral

$$T(\theta,\phi)|_{n=0 \text{ or } 1} = 2\pi abj^n \cos\left[n\left(\Delta-\Phi\right)\right] \int_0^1 R(t) J_n(ut)\, tdt \tag{A1}$$

From (16) and (17),

$$T(\theta,\phi) = I_1 \int_0^1 R(t)\, abt\, dt, \tag{A2}$$

where after substituting $x = \psi - \Phi$,

$$\begin{aligned} I_1 \;=\; & \int_0^{2\pi} \{\cos(nx)\cos\left[n\left(\Phi-\Delta\right)\right] \\ & -\sin(nx)\sin\left[n\left(\Phi-\Delta\right)\right]\} \exp\left[jut\cos x\right] dx. \end{aligned} \tag{A3}$$

Using [15] (3.915.2), and noting that the term with sine is zero because it's an odd function:

$$I_1 = 2\pi j^n \cos\left[n\left(\Phi-\Delta\right)\right] J_n(ut) \tag{A4}$$

Q.E.D.

A.2. Derivation of (30), the Space Factor of the Simplest Difference Pattern

$$T_D^{\text{norm}}|_{Q_D=\cos(\psi-\Delta)} = j\pi\cos(\Delta-\Phi)\frac{J_1(u)H_0(u)-H_1(u)J_0(u)}{u} \quad \text{(A5)}$$

From (18):

$$T_D^{\text{norm}}(\theta,\phi) = 2j\cos(\Delta-\Phi)\int_0^1 R(t)J_1(ut)tdt = \int_0^1 J_1(ut)tdt. \quad \text{(A6)}$$

[15] (6.561.1) provides

$$\int_0^1 x^v J_v(ax)\,dx = 2^{v-1}a^{-v}\pi^{\frac{1}{2}}\Gamma\left(v+\tfrac{1}{2}\right)\left[J_v(a)H_{v-1}(a)-H_v(a)J_{v-1}(a)\right], \quad \text{(A7)}$$

thus

$$T_D^{\text{norm}}(\theta,\phi) = 2j\cos(\Delta-\Phi)\left(\frac{\sqrt{\pi}}{u}\Gamma\left(\tfrac{3}{2}\right)\right)\left[J_1(u)H_0(u)-H_1(u)J_0(u)\right]. \quad \text{(A8)}$$

where $\Gamma\left(\frac{3}{2}\right) = \sqrt{\pi}/2$. Q.E.D.

A.3. Derivation of (32), the 3PS Radiation Pattern Space Factor

$$T_S^{\text{norm}}(u) = 2c\frac{J_1(u)}{u} + (1-c)\frac{2\beta^\alpha J_{\alpha+1}\left(\sqrt{u^2-\beta^2}\right)}{I_\alpha(\beta)\left(\sqrt{u^2-\beta^2}\right)^{\alpha+1}} \quad \text{(A9)}$$

From (18)

$$\begin{aligned} T_S^{\text{norm}}(\theta) &= 2\int_0^1 R(t)J_0(ut)\,tdt \\ &= 2\int_0^1 \left\{c + (1-c)\left(\sqrt{1-t^2}\right)^\alpha \frac{I_\alpha\left(\beta\sqrt{1-t^2}\right)}{I_\alpha(\beta)}\right\} J_0(ut)\,tdt \end{aligned} \quad \text{(A10)}$$

Consider first the constant term, utilizing [15] (5.52.1):

$$\text{(5.52.1):} \quad \int x^{p+1}Z_p(x)\,dx = x^{p+1}Z_{p+1}(x) \quad \text{(A11)}$$

Thereby,

$$2c\int_0^1 J_0\left(ut\right)tdt = 2c\frac{J_1\left(u\right)}{u} \tag{A12}$$

Let I_2 symbolize the second term on the RHS of (A10), utilizing [15] (6.683.2).

$$I_2 = \frac{2\left(1-c\right)}{J_\alpha\left(j\beta\right)}\int_0^1 \left(\sqrt{1-t^2}\right)^\alpha J_\alpha\left(j\beta\sqrt{1-t^2}\right)J_0\left(ut\right)tdt \tag{A13}$$

Then substitute $\sqrt{1-t^2} = \sin x$:

$$I_2 = \frac{2\left(1-c\right)}{J_\alpha\left(j\beta\right)}\int_0^{\pi/2} J_\alpha\left(j\beta\sin x\right)J_0\left(u\cos x\right)\sin^{\alpha+1}x\cos xdx \tag{A14}$$

$$(6.683.2)\text{:}\quad \int_0^{\pi/2} J_v\left(z_1\sin x\right)J_u\left(z_2\cos x\right)\sin^{v+1}x\cos^{u+1}xdx$$

$$= \frac{z_1^v z_2^u J_{v+u+1}\left(\sqrt{z_1^2+z_2^2}\right)}{\sqrt{\left(z_1^2+z_2^2\right)^{v+u+1}}} \tag{A15}$$

Thus

$$I_2 = \frac{2\left(1-c\right)}{J_\alpha\left(j\beta\right)}\frac{\left(j\beta\right)^\alpha J_{\alpha+1}\left(\sqrt{u^2-\beta^2}\right)}{\sqrt{\left(u^2-\beta^2\right)^{\alpha+1}}}$$

$$= \left(1-c\right)\frac{2\beta^\alpha J_{\alpha+1}\left(\sqrt{u^2-\beta^2}\right)}{I_\alpha\left(\beta\right)\sqrt{\left(u^2-\beta^2\right)^{\alpha+1}}}, \tag{A16}$$

Q.E.D.

A.4. Derivation of (34), the 3PS Aperture Power Integral

$$P_{\mathrm{ap}S}^{\mathrm{norm}} = c^2 + 4c\left(1-c\right)\frac{I_{\alpha+1}\left(\beta\right)}{\beta I_\alpha\left(\beta\right)} + \frac{\left(1-c\right)^2}{2\alpha+1}\left(1-\frac{I_{\alpha+1}^2\left(\beta\right)}{I_\alpha^2\left(\beta\right)}\right) \tag{A17}$$

The aperture power integral according to (23) is

$$P_{\mathrm{ap}S} = \int_0^{2\pi}\int_0^1 Q_S^2\left(t,\psi\right)abtdtd\psi, \tag{A18}$$

where

$$Q_S\left(t,\psi\right) = c + \left(1-c\right)\left(\sqrt{1-t^2}\right)^\alpha \frac{I_\alpha\left(\beta\sqrt{1-t^2}\right)}{I_\alpha\left(\beta\right)}. \tag{A19}$$

Thus

$$P_{\text{apS}}^{\text{norm}} = 2\int_0^1 \left\{ c + (1-c)\left(\sqrt{1-t^2}\right)^{\alpha} \frac{I_\alpha\left(\beta\sqrt{1-t^2}\right)}{I_\alpha(\beta)} \right\}^2 tdt. \quad \text{(A20)}$$

Let

$$P_{\text{ap}S}^{\text{norm}} \doteq c^2 + 4\frac{c(1-c)}{J_\alpha(j\beta)} I_3 + \frac{(1-c)^2}{J_\alpha^2(j\beta)} I_4, \quad \text{(A21)}$$

where

$$I_3 = \int_0^1 J_\alpha\left(j\beta\sqrt{1-t^2}\right)\left(\sqrt{1-t^2}\right)^{\alpha} tdt, \quad \text{(A22)}$$

and

$$I_4 = 2\int_0^1 J_\alpha^2\left(j\beta\sqrt{1-t^2}\right)\left(1-t^2\right)^{\alpha} tdt. \quad \text{(A23)}$$

I_3 is solved by change of variables $x = j\beta\sqrt{1-t^2}$ to reduce it to the form of (A11).

$$I_3 = \frac{1}{(j\beta)^{\alpha+2}} \int_0^{j\beta} x^{\alpha+1} J_\alpha(x)\, dx = \frac{J_{\alpha+1}(j\beta)}{j\beta} \quad \text{(A24)}$$

For I_4 let $x = 1 - t^2$ to put it into a form that Maple solves:

$$I_4 = \int_0^1 J_\alpha^2\left(j\beta\sqrt{x}\right) x^{\alpha} dx = \frac{J_\alpha^2(j\beta) + J_{\alpha+1}^2(j\beta)}{2\alpha+1} \quad \text{(A25)}$$

Q.E.D.

A.5. Derivation of (41), the 3PD Radiation Pattern Space Factor

$$\begin{aligned} T_D^{\text{norm}}(u) \;=\; & 2j\cos(\Delta-\Phi)\Big\{ c\frac{\pi}{2u}\left[J_1(u)H_0(u) - H_1(u)J_0(u)\right] \\ & + (1-c)\frac{u\beta^{\alpha} J_{\alpha+2}\left(\sqrt{u^2-\beta^2}\right)}{I_\alpha(\beta)\left(\sqrt{u^2-\beta^2}\right)^{\alpha+2}} \Big\} \end{aligned} \quad \text{(A26)}$$

From (18),

$$T_D^{\text{norm}}(\theta,\phi) = 2j\cos(\Delta-\Phi)\int_0^1 R(t) J_1(ut)\, tdt \quad \text{(A27)}$$

where

$$R_D(t) = c + (1-c)\, t \left(\sqrt{1-t^2}\right)^{\alpha} \frac{I_\alpha\left(\beta\sqrt{1-t^2}\right)}{I_\alpha(\beta)} \tag{A28}$$

The first term on the RHS with the c coefficient was derived above starting with (A5). For the second term, define

$$I_5 = \int_0^1 \left\{ t \left(\sqrt{1-t^2}\right)^{\alpha} \frac{I_\alpha\left(\beta\sqrt{1-t^2}\right)}{I_\alpha(\beta)} \right\} J_1(ut)\, t dt. \tag{A29}$$

Let $t = \sin x$:

$$I_5 = \frac{1}{j^\alpha I_\alpha(\beta)} \int_0^{\pi/2} J_1(u \sin x)\, J_\alpha(j\beta \cos x) \sin^2 x \cos^{\alpha+1} x dx \tag{A30}$$

Utilizing (A15),

$$I_5 = \frac{u\beta^\alpha J_{\alpha+2}\left(\sqrt{u^2-\beta^2}\right)}{I_\alpha(\beta)\sqrt{(u^2-\beta^2)^{\alpha+2}}} \tag{A31}$$

Q.E.D.

A.6. Derivation of (43), 3PD Matching Sum Pattern Space Factor

$$T_{|D|}^{\text{norm}}(0) = 2\left\{ \frac{c}{\pi} + (1-c)\sqrt{\frac{2}{\pi}} \frac{I_{\alpha+3/2}(\beta)}{\beta^{3/2} I_\alpha(\beta)} \right\} \tag{A32}$$

From Equation (24),

$$\begin{aligned} T_{|D|}^{\text{norm}}(0) &= \frac{1}{\pi} \int_0^{2\pi} \int_0^1 R_D(t) \left|\cos(\psi - \Delta)\right| t\, dt d\psi \\ &= \frac{4}{\pi} \int_0^1 R_D(t) t dt \qquad \text{(A33)} \\ &= \frac{4}{\pi} \int_0^1 \left\{ c + (1-c) t \left(\sqrt{1-t^2}\right)^{\alpha} \frac{I_\alpha\left(\beta\sqrt{1-t^2}\right)}{I_\alpha(\beta)} \right\} t dt \qquad \text{(A34)} \end{aligned}$$

Let $t = \cos\theta$:

$$T_{|D|}^{\text{norm}}(0) = \frac{2c}{\pi} + \frac{4(1-c)}{\pi J_\alpha(j\beta)} \int_0^{\pi/2} J_\alpha(j\beta \sin\theta) \sin^{\alpha+1}\theta \cos^2\theta d\theta \tag{A35}$$

Using [15] (6.683.6)

$$(6.683.6):\ \int_0^{\pi/2} J_u\left(a\sin\theta\right)\left(\sin\theta\right)^{u+1}\left(\cos\theta\right)^{2p+1}d\theta$$

$$2^p\Gamma\left(p+1\right)a^{-p-1}J_{p+u+1}\left(a\right) \tag{A36}$$

$$T_{|D|}^{\text{norm}}(0)=\frac{2c}{\pi}+\frac{4(1-c)}{\pi J_\alpha(j\beta)}\left[2^{\frac{1}{2}}\Gamma\left(\tfrac{3}{2}\right)(j\beta)^{-3/2}J_{\alpha+3/2}(j\beta)\right] \tag{A37}$$

Q.E.D.

A.7. Derivation of (44), the 3PD Aperture Power Integral

$$P_{\text{ap}D}^{\text{norm}}=\left\{\frac{c^2}{2}+\frac{2c\left(1-c\right)}{\beta^{3/2}}\sqrt{\frac{\pi}{2}}\frac{I_{\alpha+3/2}\left(\beta\right)}{I_\alpha\left(\beta\right)}+\frac{\left(1-c\right)^2}{2}\left[\frac{1-\dfrac{I_{\alpha+1}^2(\beta)}{I_\alpha^2(\beta)}}{2\alpha+1}-\frac{\beta^{2\alpha}{}_2F_3\left(\begin{matrix}[2\alpha+2,\alpha+1/2]\,;\\ [2\alpha+1,2\alpha+3,\alpha+1]\,;\end{matrix}\beta^2\right)}{2^{2\alpha+1}(\alpha+1)\Gamma^2(\alpha+1)I_\alpha^2(\beta)}\right]\right\} \tag{A38}$$

The aperture power integral according to (23) is

$$P_{\text{ap}D}=\int_0^{2\pi}\int_0^1 Q_D^2\left(t,\psi\right)abt\,dtd\psi, \tag{A39}$$

where

$$Q_D(t,\psi)=\cos(\psi-\Delta)\left\{c+(1-c)t\left(\sqrt{1-t^2}\right)^\alpha\frac{I_\alpha\left(\beta\sqrt{1-t^2}\right)}{I_\alpha(\beta)}\right\}. \tag{A40}$$

Thus

$$P_{\text{ap}D}^{\text{norm}}=\int_0^1\left\{c+\left(1-c\right)t\left(\sqrt{1-t^2}\right)^\alpha\frac{I_\alpha\left(\beta\sqrt{1-t^2}\right)}{I_\alpha\left(\beta\right)}\right\}^2 tdt. \tag{A41}$$

Let

$$P_{\text{ap}D}^{\text{norm}}\doteq\frac{c^2}{2}+2\frac{c\left(1-c\right)}{J_\alpha\left(j\beta\right)}I_6+\frac{\left(1-c\right)^2}{2J_\alpha^2\left(j\beta\right)}I_7, \tag{A42}$$

where

$$I_6=\int_0^1 J_\alpha\left(j\beta\sqrt{1-t^2}\right)\left(\sqrt{1-t^2}\right)^\alpha t^2dt, \tag{A43}$$

and

$$I_7 = 2\int_0^1 J_\alpha^2\left(j\beta\sqrt{1-t^2}\right)\left(1-t^2\right)^\alpha t^3 dt. \tag{A44}$$

For I_6 let $x = \sqrt{1-t^2}$ to yield a form that Maple and Mathematica will solve:

$$I_6 = \int_0^1 J_\alpha\left(j\beta x\right) x^{\alpha+1}\sqrt{1-x^2}dx = \sqrt{\frac{\pi}{2}}\frac{J_{\alpha+3/2}\left(j\beta\right)}{\left(j\beta\right)^{3/2}}. \tag{A45}$$

For I_7 let $x = 1-t^2$:

$$I_7 = \int_0^1 x^\alpha J_\alpha^2\left(j\beta\sqrt{x}\right)dx - \int_0^1 x^{\alpha+1}J_\alpha^2\left(j\beta\sqrt{x}\right)dx \doteq I_8 - I_9 \tag{A46}$$

From Maple:

$$I_8 = \int_0^1 x^\alpha J_\alpha^2\left(j\beta\sqrt{x}\right)dx = \frac{J_\alpha^2\left(j\beta\right) + J_{\alpha+1}^2\left(j\beta\right)}{2\alpha+1} \tag{A47}$$

Maple:

$$I_9 = \frac{\left(j\beta\right)^{2\alpha}{}_2F_3\left(\left[2\alpha+2, \alpha+\frac{1}{2}\right]; [2\alpha+1, 2\alpha+3, \alpha+1]; \beta^2\right)}{2^{2\alpha+1}\left(\alpha+1\right)\Gamma^2\left(\alpha+1\right)} \tag{A48}$$

Q.E.D.

A.8. Derivation of (48), the Slope of the Difference Pattern

$$D_{\text{slope}}^{\text{norm}} \doteq \left.\frac{dT_D^{\text{norm}}(u)}{du}\right|_{u=0} = 2j\cos(\Delta-\Phi)\left\{\frac{c}{6} + \frac{(1-c)I_{\alpha+2}(\beta)}{\beta^2 I_\alpha(\beta)}\right\} \tag{A49}$$

Recalling (41):

$$\begin{aligned}\frac{T_D^{\text{norm}}(u)}{2j\cos\left(\Delta-\Phi\right)} \;=\; &\left\{c\frac{\pi}{2u}\left[J_1\left(u\right)H_0\left(u\right) - H_1\left(u\right)J_0\left(u\right)\right]\right.\\ &\left. + \left(1-c\right)\frac{u\beta^\alpha J_{\alpha+2}\left(\sqrt{u^2-\beta^2}\right)}{I_\alpha\left(\beta\right)\left(\sqrt{u^2-\beta^2}\right)^{\alpha+2}}\right\}\end{aligned} \tag{A50}$$

Equation (26) defines the slope:

$$D_{\text{slope}}^{\text{norm}} \doteq \left.\frac{dT_D^{\text{norm}}\left(u\right)}{du}\right|_{u=0} \tag{A51}$$

Using either Maple, Mathematica or working out the arithmetic by hand, noting that $\lim_{x\to 0} H_0(x)/x = 2/\pi$ and $\lim_{x\to 0} H_1(x)/x^2 = 2/(3\pi)$, yields the given result.

REFERENCES

1. Collin, R. E. and F. J. Zucker, *Antenna Theory, Volume 2*, McGraw-Hill Companies, New York, 1969.
2. Duan, D.-W. and Y. Rahmat-Samii, "A generalized three-parameter (3-P) aperture distribution for antenna applications," *IEEE Transactions on Antennas and Propagation*, Vol. 40, No. 6, 697–713, 1992.
3. Hansen, R. C., "Array pattern control and synthesis," *Proceedings of the IEEE*, Vol. 80, No. 1, 141–151, 1992.
4. Elliott, R. S., *Antenna Theory and Design,* Englewood Cliffs, New Jersey, 1981.
5. Kennedy, J. and R. Eberhart, "Particle swarm optimization," *IEEE International Conference on Neural Networks Proceedings*, Vol. 4, 1942–1948, 1995.
6. Robinson, J. and Y. Rahmat-Samii, "Particle swarm optimization in electromagnetics," *IEEE Transactions on Antennas and Propagation*, Vol. 52, No. 2, 397–407, Feb. 2004.
7. Xu, S., Y. Rahmat-Samii, and D. Gies, "Shaped-reflector antenna designs using particle swarm optimization: An example of a direct-broadcast satellite antenna," *Microwave and Optical Technology Letters*, Vol. 48, No. 7, 1341–1347, 2006.
8. Yen, G. G. and W.-F. Leong, "Dynamic multiple swarms in multiobjective particle swarm optimization," *IEEE Transactions on Systems, Man and Cybernetics, Part A: Systems and Humans*, Vol. 39, No. 4, 890–911, 2009.
9. Goudos, S. K., Z. D. Zaharis, D. G. Kampitaki, I. T. Rekanos, and C. S. Hilas, "Pareto optimal design of dual-band base station antenna arrays using multi-objective particle swarm optimization with fitness sharing," *IEEE Transactions on Magnetics*, Vol. 45, No. 3, 1522–1525, 2009.
10. Chen, M., "Second generation particle swarm optimization," *IEEE Congress on Evolutionary Computation, (IEEE World Congress on Computational Intelligence), CEC 2008*, 90–96, 2008.
11. Balanis, C., *Advanced Engineering Electromagnetics,* Wiley, 1989.
12. Schelkunoff, S. A., "Some equivalence theorems of electromagnetics and their application to radiation problems," *Bell System Technical Journal*, Vol. 15, No. 1, 92–112, 1936.
13. Koffman, I., "Feed polarization for parallel currents in reflectors generated by conic sections," *IEEE Transactions on Antennas and Propagation*, Vol. 14, No. 1, 37–40, 1966.

14. Ludwig, A., "The definition of cross polarization," *IEEE Transactions on Antennas and Propagation*, Vol. 21, No. 1, 116–119, Jan. 1973.
15. Gradshteyn, I. S. and I. M. Ryzhik, *Table of Integrals, Series and Products*, 2nd Edition, Academic Press Inc., 1980.
16. Schelkunof, S. A., "A mathematical theory of linear arrays," *Bell System Technical Journal*, Vol. 22, No. 1, 80–107, Jan. 1943.
17. Taylor, T. T., "Design of circular apertures for narrow beamwidth and low sidelobes," *IRE Transactions on Antennas and Propagation*, Vol. 8, No. 1, 17–22, 1960.
18. Bayliss, E. T., "Design of monopulse antenna difference patterns with low sidelobes," *Bell System Technical Journal*, Vol. 47, No. 5, 623–650, 1968.
19. Mostaghim, S. and J. Teich, "Covering Pareto-optimal fronts by subswarms in multi-objective particle swarm optimization," *Congress on Evolutionary Computation, CEC2004*, Vol. 2, 1404–1411 2004.
20. Jin, Y. and B. Sendhoff, "Pareto-based multiobjective machine learning: An overview and case studies," *IEEE Transactions on Systems, Man, and Cybernetics, Part C: Applications and Reviews*, Vol. 38, No. 3, 397–415, May 2008.
21. Densmore, A., Y. Rahmat-Samii, and G. Seck, "Corrugated-conical horn analysis using aperture field with quadratic phase," *IEEE Transactions on Antennas and Propagation*, Vol. 59, No. 9, 3453–3457, Sep. 2011.
22. Guo, Y. and N. Lin, "A three-parameter distribution for difference pattern," *Antennas and Propagation Society International Symposium, AP-S. Digest*, Vol. 3, 1594–1597, 1993.
23. Yang, X.-S., *Introduction to Mathematical Optimization: From Linear Programming to Metaheuristics,* Cambridge International Science Publishing, 2008.
24. Dorigo, M., M. Birattari, and T. Stutzle, "Ant colony optimization," *IEEE Computational Intelligence Magazine*, Vol. 1, No. 4, 28–39, 2006.
25. Gregory, M. D., Z. Bayraktar, and D. H. Werner, "Fast optimization of electromagnetic design problems using the covariance matrix adaptation evolutionary strategy," *IEEE Transactions on Antennas and Propagation*, Vol. 59, No. 4, 1275–1285, 2011.
26. Rahmat-Samii, Y. and E. Michielssen, *Electromagnetic Optimization by Genetic Algorithms,* J. Wiley, 1999.

27. Karimkashi, S. and A. A. Kishk, "Invasive weed optimization and its features in electromagnetics," *IEEE Transactions on Antennas and Propagation*, Vol. 58, No. 4, 1269–1278, Apr. 2010.
28. Wang, Y., W. Yan, and G. Zhang, "Adaptive simulated annealing for the optimal design of electromagnetic devices," *IEEE Transactions on Magnetics*, Vol. 32, No. 3, 1214–1217, 1996.
29. Fanni, A., A. Manunza, M. Marchesi, and F. Pilo, "Tabu search metaheuristics for global optimization of electromagnetic problems," *IEEE Transactions on Magnetics*, Vol. 34, No. 5, 2960–2963, 1998.
30. Azaro, R., F. De Natale, M. Donelli, E. Zeni, and A. Massa, "Synthesis of a prefractal dual-band monopolar antenna for GPS applications," *IEEE Antennas and Wireless Propagation Letters*, Vol. 5, No. 1, 361–364, 2006.
31. Azaro, R., G. Boato, M. Donelli, A. Massa, and E. Zeni, "Design of a prefractal monopolar antenna for 3.4–3.6 GHz Wi-Max band portable devices," *IEEE Antennas and Wireless Propagation Letters*, Vol. 5, No. 1, 116–119, 2006.
32. Donelli, M., R. Azaro, F. G. B. De Natale, and A. Massa, "An innovative computational approach based on a particle swarm strategy for adaptive phased-arrays control," *IEEE Transactions on Antennas and Propagation*, Vol. 54, No. 3, 888–898, 2006.
33. "Code of Federal Regulations, Title 47 Telecommunications, Chapter 1 Federal Communications Commission, Subchapter B Common Carrier Services, Part 25 Satellite Communications, Subpart C Technical Standards, Section 25.209 Antenna Performance Standards," US Government Printing Office.
34. Rahmat-Samii, Y., "On the question of computation of the dyadic Green's function at the source region in waveguides and cavities (short papers)," *IEEE Transactions on Microwave Theory and Techniques*, Vol. 23, No. 9, 762–765, 1975.